



PCCP

**A Molecular Dynamics Investigation Of Actinyl-Ligand Speciation In Aqueous Solution**

Journal:	<i>Physical Chemistry Chemical Physics</i>
Manuscript ID	CP-ART-03-2018-001944.R1
Article Type:	Paper
Date Submitted by the Author:	08-May-2018
Complete List of Authors:	Newcomb, Ken; University of Notre Dame, Department of Chemical and Biomolecular Engineering Tiwari, Surya; U. S. Department of Energy, National Energy Technology Laboratory; AECOM Rai, Neeraj; Mississippi State University, Dave C. Swalm School of Chemical Engineering Maginn, Edward; University of Notre Dame, Department of Chemical and Biomolecular Engineering

SCHOLARONE™  
Manuscripts

Cite this: DOI: 10.1039/xxxxxxxxxxx

# A Molecular Dynamics Investigation Of Actinyl-Ligand Speciation In Aqueous Solution<sup>†</sup>

Ken Newcomb,<sup>\*a</sup> Surya Prakash Tiwari,<sup>bc</sup> Neeraj Rai,<sup>d</sup> and Edward J. Maginn<sup>a</sup>Received Date  
Accepted Date

DOI: 10.1039/xxxxxxxxxxx

www.rsc.org/journalname

Actinyl ions ( $\text{AnO}_2^{n+}$ ), the form in which actinides are commonly found in aqueous solution, are important species in the nuclear fuel cycle. These ions can form stable complexes with ionic ligands such as  $\text{OH}^-$ ,  $\text{NO}_3^-$ ,  $\text{Cl}^-$ , and even other actinyl ions in the aqueous phase. Knowledge of the relative stabilities of these complexes is important for the efficient design of separation processes used in recycling. These complexes also play a major role in the formation of actinide nanoclusters. A quantitative treatment of the stability of these actinyl ion complexes is therefore warranted. In the present work, molecular dynamics (MD) simulations have been performed to calculate the potential of mean force (PMF) between two actinyl ions ( $\text{UO}_2^{2+}$  and  $\text{NpO}_2^+$ ) and various ligands ( $\text{F}^-$ ,  $\text{Cl}^-$ ,  $\text{OH}^-$ ,  $\text{NO}_3^-$ ,  $\text{SO}_4^{2-}$ ,  $\text{CO}_3^{2-}$ ,  $\text{Na}^+$ , and  $\text{H}_2\text{O}$ ) in explicitly-modeled aqueous solution. Equilibrium constants were calculated from the PMFs, and are consistent with experimental trends. Dication actinyls show stronger affinity for anions compared to monocation actinyls, whereas the opposite is true for cation-cation interactions between actinyls. Finally, the dynamics of actinyl-ligand contact ion pair (CIP) dissociation were characterized by calculating rate constants from transition state theory. The transmission coefficient, a dynamical correction factor used to correct for reaction barrier recrossing, was calculated for each actinyl-ligand CIP dissociation event.

## 1 Introduction

The International Union of Pure and Applied Chemistry (IUPAC) defines speciation as the distribution of an element amongst the defined chemical species in a system. Understanding the speciation of metal ions in the aqueous phase is important, as it makes the basis for predicting the behavior of metal ions in the environment, biological systems, analytical chemistry, extractive metallurgy, and other chemical processes<sup>1–3</sup>. The speciation of actinyl ions in the aqueous phase is critical for a fundamental understanding of the behavior of nuclear materials. For example, in the event that nuclear waste is accidentally discharged to an aquifer, actinyl ions will form complexes with various ionic ligands naturally found in water such as  $\text{Na}^+$ ,  $\text{Cl}^-$ ,  $\text{OH}^-$ ,  $\text{F}^-$ ,  $\text{NO}_3^-$ ,  $\text{CO}_3^{2-}$  and  $\text{SO}_4^{2-}$ , thereby affecting the mobility of discharged nuclear waste in the environment. Furthermore, the recycling of spent nuclear

fuel and stored nuclear waste often requires contact with water and dissolved ions. A knowledge of the thermodynamics and kinetics of complex formation is needed for rationally choosing the appropriate ligands in designing efficient separation processes. Finally, ionic ligands also play a very important role in actinide nanocluster formation<sup>4</sup>.

Several *ab initio* calculations<sup>3,5–14</sup> and classical molecular dynamics (MD) simulation studies<sup>12,15–17</sup> have been conducted to examine the interaction between the uranyl ion and various ligands such as water, nitrate, acetonitrile, fluoride, and chloride. In these studies, structural properties such as the radial distribution function and uranyl ion-ligand bond lengths were calculated, in addition to binding energies between uranyl ion and ligands. Vukovic et al.<sup>3</sup> used density functional theory (DFT) and the integral equation formalism/polarizable continuum model (IEF-PCM) to predict the stability constants ( $K_1$ ) for the formation of 1:1 uranyl-ligand aqueous complexes for 18 different negative oxygen and oxime-based donor ligands. The theoretical calculations correctly determined the order of  $\text{UO}_2^{2+}$ -ligand stability but significantly overestimated the absolute  $\log K_1$  values because of the inaccurate modeling of ion solvation free energy. Dang et al.<sup>18</sup> developed a polarizable force field for the study of water exchange around the uranyl ion. Transition state theory (TST) was applied to calculate the rate of water exchange as a function of pressure.

Although previous studies of uranyl ion-ligand interactions pro-

<sup>a</sup> Department of Chemical and Biomolecular Engineering, 182 Fitzpatrick Hall, University of Notre Dame, Notre Dame, IN 46556, USA. E-mail: ed@nd.edu;  
Fax: +1 574 631 8366; Tel: +1 574 631 5687

<sup>b</sup> U. S. Department of Energy, National Energy Technology Laboratory, Pittsburgh, PA 15236, USA

<sup>c</sup> AECOM, South Park, PA 15129, USA

<sup>d</sup> Dave C. Swalm School of Chemical Engineering, Mississippi State University, Mississippi State, MS, USA 39762

<sup>†</sup> Electronic Supplementary Information (ESI) available: [details of any supplementary information available should be included here]. See DOI: 10.1039/cXCP00000x/

vide a very good insight on their association, a knowledge of the process of complex formation along with an identification of the topologies for different extents of complexation will be more helpful in understanding the association. Furthermore, since molecular dynamics can accurately model solvation and requires less computational power than DFT, determining stability constants from MD simulations is an attractive proposition.

In our previous work<sup>19–22</sup>, we developed force field parameters for actinyl ions in water. We further calculated several thermodynamic properties of actinyl ions using MD simulations. In addition, we studied the mechanism and kinetics of water's exchange into the actinyl ion's solvation shells. In the present work, we investigate the association between actinyl ions and various ligands *viz.*, Na<sup>+</sup>, Cl<sup>-</sup>, OH<sup>-</sup>, F<sup>-</sup>, NO<sub>3</sub><sup>-</sup>, CO<sub>3</sub><sup>2-</sup>, SO<sub>4</sub><sup>2-</sup>, and H<sub>2</sub>O. We choose divalent cation-UO<sub>2</sub><sup>2+</sup> and monovalent cation-NpO<sub>2</sub><sup>+</sup> for this study, since UO<sub>2</sub><sup>2+</sup> and NpO<sub>2</sub><sup>+</sup> ions are the most commonly found states of U and Np in water. The adaptive biasing force (ABF) algorithm<sup>23</sup> has been used to calculate the potential of mean force (PMF), which represents the free energy change as a function of distance between actinyl ion and ligand in solution. Using the PMF calculations, stability constants were computed and compared with experimental results. A detailed structural analysis was performed by calculating the spatial distribution functions for the attachment of anionic ligands to actinyl ions. Finally, the TST dissociation rate constants were calculated for a variety of ligands. By performing simulations in the constrained reaction coordinate ensemble<sup>24</sup>, a dynamical correction factor to TST known as the transmission coefficient was calculated for each dissociation event. This factor allows for the calculation of the true ligand dissociation rate by accounting for barrier recrossing.

## 2 Theory and Computational Details

### 2.1 Force Field Development

All calculations were performed using a classical force field. The non-bonded interactions were modeled with Lennard-Jones (LJ) and Coulomb potentials, while bond stretching and angle bending were modeled with harmonic functions, as in our previous studies. Force field parameters (FFPs) for interactions between the atoms of actinyl ions and SPC/E water<sup>25</sup> ( $\sigma_{\text{AnOw}}$ ,  $\epsilon_{\text{AnOw}}$ ,  $\sigma_{\text{OAnOw}}$ ,  $\epsilon_{\text{OAnOw}}$ , and the partial atomic charges of the actinyl ions) were also taken from our previous work.<sup>20</sup> To obtain the interaction between atoms of the actinyl ion and ligand of interest, the Lorentz-Berthelot (LB) combining rule was used<sup>26</sup>. This methodology was used to calculate the  $\sigma_{ii}$  and  $\epsilon_{ii}$  for the An-An and OAn-OAn interactions; the parameters are shown in Table 1.

**Table 1** AnO<sub>2</sub><sup>+</sup> - AnO<sub>2</sub><sup>+</sup> LJ interaction parameters, generated by LB mixing rules. Atom centers are shown in bold type.

type	$\sigma_{ii}$ (nm)	$\epsilon_{ii}$ (kJ/mol)
<b>An-An</b>	0.295	0.530
<b>OAn-OAn</b>	0.383	0.057

The accuracy of these LJ parameters generated by LB combining rules was verified by quantum mechanical (QM) calculations.

The classical potential energy surfaces (PESs) generated from the use of the combining-rule overlap reasonably well with the QM PESs, as shown in Fig. 1. The classical PESs are slightly more repulsive at intermolecular distances shorter than 0.4 nm. Fortunately, configurations with such short distances are very repulsive and have an extremely low probability of occurrence. Therefore, the use of the LB combining rule to produce these parameters is justified.

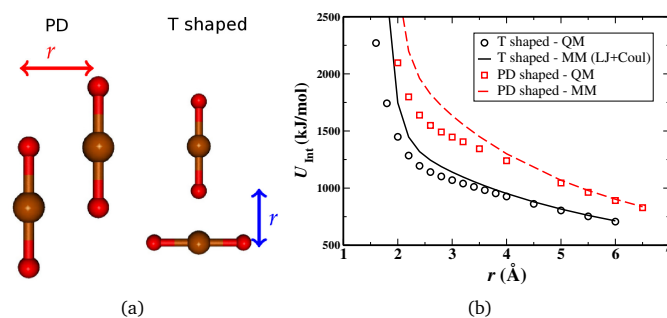


**Fig. 1** (a) Configurations used to generate potential energy surfaces. (b) Comparison between potential energy surfaces obtained from QM calculation and classical potential with parameters obtained using LB combining rules for UO<sub>2</sub><sup>2+</sup>-UO<sub>2</sub><sup>2+</sup> interaction for different configurations.

Given  $\sigma_{ii}$  and  $\epsilon_{ii}$  for atoms of the actinyl ion, the LB combining rule was further used to obtain the interaction between the actinyl ion and various ligands. FFPs for various ligands were obtained from the literature and are well tested for their use in aqueous phase simulations. The parameters used in this work can be found in the Supplementary Information (SI).

As done previously, a QM PES was generated for each actinide-ligand pair to compare against the classical PES generated by applying combining rules. An overbinding between the actinyl-ligand pair was observed. We attribute this overbinding to the use of an unsolvated ligand. We have therefore chosen to use the classical PES for all calculations. For completeness, the process of fitting the QM data to LJ plus Coulombic functional form, along with the generated parameters, can be found in the SI.

### 2.2 Potential of Mean Force Calculations

The potential of mean force (PMF),  $W(r)$ <sup>27–30</sup>, gives the free energy change along some reaction coordinate  $r$ , and is defined from the average distribution function  $\langle \rho(r) \rangle$

$$W(r) = -k_B T \ln[\langle \rho(r) \rangle] + C \quad (1)$$

$$\text{where } \langle \rho(r) \rangle = \frac{\int d\mathbf{q} \delta(r'(\mathbf{q}) - r) e^{-U(\mathbf{q})/k_B T}}{\int d\mathbf{q} e^{-U(\mathbf{q})/k_B T}}, \quad (2)$$

$k_B$  is the Boltzmann constant,  $T$  is the absolute temperature,  $U(\mathbf{q})$  is the total energy of the system as a function of coordinates  $\mathbf{q}$ ,  $r'(\mathbf{q})$  is a function of a few particular degrees of freedom in the system such as distance or angle, and  $C$  is an arbitrary constant. The PMF quantifies the relative probabilities of different states. It is thus useful in describing relative stabilities of different conformational states, the attraction between two species, and transi-

tion probabilities<sup>31</sup>. In this study,  $r$  is defined as the actinyl-ligand distance.

The calculation of  $W(r)$  or  $\langle\rho(r)\rangle$  from a standard MD simulation is often impractical, since the presence of large free energy barriers along  $r$  may prevent an accurate sampling of the configurational space within the available computer time.<sup>32</sup> As a result, a PMF obtained in this way will have poor statistics compared to a PMF obtained from an enhanced sampling technique such as ABF<sup>23</sup>. ABF accrues a running estimate of the the average force between the uranyl-ligand pair, and applies an equal and opposite biasing force. This average force  $\bar{F}$  is equal to the derivative of the potential of mean effective force (PMEF), denoted  $W_{eff}(r)$ :

$$\bar{F} = \frac{d}{dr}W_{eff}(r) = \frac{d}{dr}A(r;T,V,N) \quad (3)$$

where  $A$  is the Helmholtz free energy. The PMEF is related to the PMF through a entropic correction factor, which accounts for the increase of configurations on a sphere of a radius  $r$ :

$$W(r) = W_{eff}(r) + 2k_B T \ln(r) \quad (4)$$

Finally, the resulting PMF was calibrated with the screened Coulomb potential, discussed in a later section.

### 2.2.1 PMF Calculation using ABF

In this work, the following procedures were adapted for obtaining the PMF between an actinyl ion and a ligand in the aqueous phase as a function of distance between their center of masses,  $r$ . A cubic box with  $\sim 3.12$  nm edge lengths was used in all PMF simulations. One actinyl ion, the ligand of interest, and 1000 SPC/E water molecules were placed inside the box. Periodic boundary conditions were incorporated in all three directions. Long-range electrostatic forces were handled using particle-mesh Ewald<sup>33,34</sup> (PME). A switch function was used for the LJ and Coulombic interactions, which is turned on at 1 nm to make the force smoothly go to zero at a distance of 1.2 nm. MD simulations were carried out in the NVT ensemble using the density computed from NPT simulation at 1 atm and 298.15 K. A calculation consists of four independent ABF simulations (“walkers”), each running for 50 nanoseconds. 300 histogram bins were used to store the average force along the collective variable (CV). The biasing force was turned on gradually using a linear ramp over 500 time steps to avoid instability. Three independent calculations of the PMF were computed to estimate error from the standard deviation.

### 2.3 Calculation of Stability Constants ( $K_a$ )

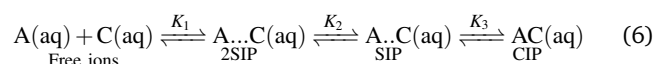
One fundamental characterization of 1:1 metal-ligand binding is the stability constant (also referred to as association, formation, or equilibrium constant). This thermodynamic quantity gives the relative presence of one metal-ligand binding state to another. In the present work, we will use the term “stability constant”, following the convention adopted by the Nuclear Energy Agency (NEA) and others<sup>3,35,36</sup>.

The equilibrium reaction in dilute aqueous solution between two free species  $A$  and  $C$  to form an associated complex  $A:C$  can

be denoted by:



To simplify the formulation, we ignore polycluster formation. This assumption is later justified: the addition of more than one ligand to the actinyl ion is associated with a large free energy penalty. The association process denoted by the above equation can be divided into a multi-step mechanism given in terms of contact ion pair (CIP), solvent shared ion pair (SIP) and solvent separated ion pair (2SIP) to form a combined associated complex<sup>29,37</sup>, and can be represented as:



The concentration of combined association complex  $A:C$  can be written as the sum of individual concentrations of CIP, SIP and 2SIP:

$$\underset{\text{Associated}}{A : C(\text{aq})} = \underset{2\text{SIP}}{A\dots C(\text{aq})} + \underset{\text{SIP}}{A..C(\text{aq})} + \underset{\text{CIP}}{AC(\text{aq})} \quad (7)$$

Equilibrium constants, in practice, are defined by the ratio of their concentrations rather than their activities for dilute solutions. The equilibrium constants,  $K_a$ ,  $K_1$ ,  $K_2$  and  $K_3$ , defined by the equilibrium reactions in Eq. 5 and Eq. 6 are given by:

$$K_a = \frac{[A : C]}{[A][C]} \quad (8a)$$

$$K_1 = \frac{[A\dots C]}{[A][C]} \quad (8b)$$

$$K_2 = \frac{[A..C]}{[A\dots C]} \quad (8c)$$

$$K_3 = \frac{[AC]}{[A..C]} \quad (8d)$$

where square bracket denotes the concentration. It should be noted that in some literature,  $\beta$  is used to denote overall association constant  $K_a$ , and  $K_i$  is used for the consecutive or stepwise formation constant. However, in the present work, we will use the notations given in Eq. 8.

For two species  $A$  and  $C$  in an aqueous phase, the intermolecular distance between them can be used to identify free, overall associated, CIP, SIP, and 2SIP states. The limits of these distances can be determined from a PMF plot as shown schematically in Fig. 2. Let's examine Fig. 2 from the left. The region containing the first local minimum represents the CIP, bounded by  $r_0$ , and  $r_1$ .  $r_0$  is identified by the closest actinyl-ligand distance sampled, and in practice, the equilibrium constant calculation is insensitive to this value.  $r_1$  is identified by the first local maximum in the PMF. The SIP is represented by the second minimum and is bounded by the local maxima  $r_1$  and  $r_2$ , while the 2SIP is represented by the third minimum and bounded by the local maxima  $r_2$  and  $r_3$ .

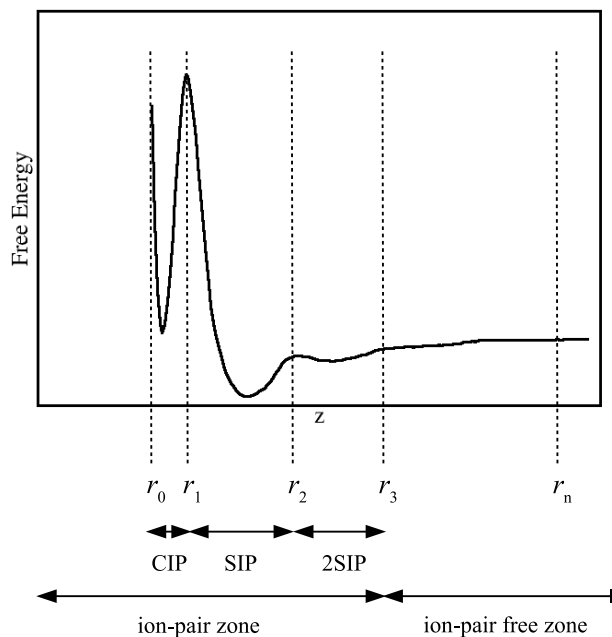


**Fig. 2** Schematic representation for definitions of various ion-pairs zones.

The entire region from bounded to the left of  $r_3$  is considered as an associated complex, and the species A and C, separated by a distance more than  $r_3$ , are considered as free or dissociated.  $r_n$  is the distance at which the PMF is calibrated to the value of the screened Coulomb potential, explained below.

Taking Bjerrum's approach<sup>37,38</sup>, the equilibrium constants for infinitely dilute solutions can be obtained from the potential of mean force profiles. They are given by the following expressions,<sup>29,37,39–41</sup> where integrations are performed over the regions containing ion pairing species:

$$K_a = 4\pi C \int_{r_0}^{r_3} \exp\left[\frac{-W(r)}{k_B T}\right] r^2 dr \quad (9)$$

$$K_1 = 4\pi C \int_{r_2}^{r_3} \exp\left[\frac{-W(r)}{k_B T}\right] r^2 dr \quad (10)$$

$$K_2 = \frac{\int_{r_1}^{r_2} \exp\left[\frac{-W(r)}{k_B T}\right] r^2 dr}{\int_{r_2}^{r_3} \exp\left[\frac{-W(r)}{k_B T}\right] r^2 dr} \quad (11)$$

$$K_3 = \frac{\int_{r_0}^{r_1} \exp\left[\frac{-W(r)}{k_B T}\right] r^2 dr}{\int_{r_1}^{r_2} \exp\left[\frac{-W(r)}{k_B T}\right] r^2 dr} \quad (12)$$

$C$  is simply the conversion factor from cubic nm per molecule to cubic decimeters per mole. The exponential terms in the above equations are radial distribution functions, and the overall integrals are number integrals or cumulative distribution functions for the interaction between two species A and C. A rigorous derivation of the above equations can be found in the paper by

Chialvo et al.<sup>39</sup>. An accurate calibration of the PMF is needed to calculate precise association constants. In the literature, calibration is done in the following ways. A simple way is to make the PMF equal to zero at a long distance.<sup>42,43</sup> However, interactions between ions won't be zero at these distances due to the long range nature of the Coulomb potential. The second method is to make the PMF equal to the Coulomb potential ( $\frac{q_1 q_2 e^2}{4\pi\epsilon_0\epsilon_r}$ ) at long distance.<sup>44</sup> The third method is to calculate the free energy at a given distance and then adjust PMF accordingly<sup>40</sup>. The fourth method, adopted in this work, is to make the PMF equal to the screened Coulomb potential ( $\frac{q_1 q_2 e^2}{4\pi\epsilon_0\epsilon_r} \frac{e^{-\kappa r}}{r}$ ) from Debye-Hückel theory<sup>45</sup> at long distance,  $r_n = 1.0$  nm.<sup>29,46,47</sup> This method was chosen based on a compromise of speed vs. accuracy.  $\kappa^{-1}$  is the Debye decay length<sup>45</sup>, and is given by

$$\kappa = [\epsilon_0\epsilon_r k_B T / \Sigma e^2 (z^k)^2 n_b^k]^{1/2} \quad (13)$$

where  $n_b^k$  is the average (bulk) concentration of species  $k$ , and a dielectric constant of  $\epsilon_r = 76$  for SPC/E water<sup>48</sup> was used.

#### 2.4 Determination of Dissociation Rate Constants

The interaction between an actinyl ion and ligand, forming a CIP, can be further quantified by dissociation rate constants. In theory, the rate of ligand dissociation can be directly extracted from an MD trajectory. However, for events that occur on timescales inaccessible by MD, one can apply classical transition state theory (TST)<sup>31,49</sup> to calculate the rate. The critical assumption of TST is that each time the reactants pass through the transition state, they proceed to products and thermalize in the product state before recrossing again. The transition states are identified by the maxima in PMF, separating one actinide-ligand binding state from the next. According to the TST formalism, the rate constant is the product of the average (forward) velocity of the actinide-ligand pair and the probability of being at the transition state:

$$k^{\text{TST}} = \langle \dot{r}(0) \theta[\dot{r}(0)] \rangle_{r^\ddagger} p(r^\ddagger) \quad (14)$$

where  $r^\ddagger$  is the location of the transition state,  $\dot{r}(0)$  is the rate of change of distance between the actinide and ligand at  $t = 0$ ,  $\theta$  is the Heaviside function, and  $p(r^\ddagger)$  is the probability of achieving the transition state. The angle brackets  $\langle \dots \rangle_{r^\ddagger}$  indicate a canonical ensemble average over all possible configurations where the system is found at the transition state. The first term, the average rate of displacement of the actinide-ligand pair, was calculated using Maxwell-Boltzmann statistics. The second term was calculated from the PMF. Using the two terms,  $k^{\text{TST}}$  is:

$$k^{\text{TST}} = \sqrt{\frac{k_B T}{2\pi\mu}} \frac{r^{\ddagger 2} e^{-\beta W(r^\ddagger)}}{\int_0^{r^\ddagger} r^2 e^{-\beta W(r)} dr} = \sqrt{\frac{k_B T}{2\pi\mu}} \frac{e^{-\beta W_{\text{eff}}(r^\ddagger)}}{\int_0^{r^\ddagger} e^{-\beta W_{\text{eff}}(r)} dr} \quad (15)$$

where  $\mu$  is the reduced mass of the actinyl-ligand pair.

It is clear that this formulation will overpredict the rate of ligand dissociation, since all forward moving trajectories do *not* directly proceed to products, but recross the transition state one or more times before thermalizing in the product well. We can cor-

rect this assumption by the introduction of a dynamical correction factor known as the transmission coefficient<sup>50</sup>, denoted by  $\kappa$ :

$$\kappa^{\text{actual}} = \kappa k^{\text{TST}} \quad (16)$$

While a plethora of expressions exist for the calculation of the transmission coefficient, the effective positive flux (EPF) method is a particularly robust and fast-converging method<sup>51</sup>. In essence, the EPF method ensures that only true  $A \rightarrow B$  events are counted, and only counted once in the case of multiple barrier passes. The transmission coefficient  $\kappa$  is calculated from the plateau value of the normalized reactive flux,  $k(t)$ <sup>31</sup>, which is computed in the constrained reaction coordinate ensemble<sup>24</sup>. The expression is given by<sup>49,52–55</sup>

$$k(t) = \frac{\langle \dot{r}(0)\theta[\dot{r}(0)]\chi[-t]\theta[r(t) - r^\ddagger] \rangle_{r^\ddagger}}{\langle \dot{r}(0)\theta[\dot{r}(0)] \rangle_{r^\ddagger}} \quad (17)$$

The function  $\chi(-t)$  returns 0 if the backwards trajectory recrosses the transition state between  $t = 0$  and  $t = -t$ , and returns 1 otherwise. To calculate the transmission coefficient, 2000 independent configurations were generated with the reaction coordinate (the actinide-ligand distance) constrained to the transition state. The constraint was then released, velocities were assigned according to the Maxwell-Boltzmann distribution, and the trajectories were followed forwards and backwards in time for 4 ps.

As a final remark, for a reaction that occurs without any barrier recrossing, the normalized reactive flux will be unity for all time.

## 2.5 Polyionic Association Study

To explore the possibility of multiple ligands binding to the actinyl, the  $\text{UO}_2^{2+}/\text{Cl}^-$  simulation was performed with four  $\text{Cl}^-$  ligands. We wished to understand the free energy change as a function of  $\text{Cl}^-$  coordination around the uranyl ion. From this information, the most probable actinyl-ligand state could be determined. Coordination number is a discrete variable, while ABF relies on continuous, differentiable CVs. Therefore, a smooth switching function was used to differentiate between different actinyl-ligand binding states.<sup>56,57</sup> The switching function used in this study,  $s_{ij}$ , is defined as:

$$s_{ij} = \frac{1 - \left(\frac{r_{ij} - d_0}{r_0}\right)^n}{1 - \left(\frac{r_{ij} - d_0}{r_0}\right)^m} \quad (18)$$

where  $r_{ij}$  is the distance between the uranyl ion and the  $j$ th  $\text{Cl}^-$ , and  $d_0$ ,  $r_0$ ,  $n$ , and  $m$  are free parameters. These parameters are chosen such that  $s_{ij}$  is equal to 1 when the  $\text{Cl}^-$  is coordinating the uranyl ion, and 0 when the  $\text{Cl}^-$  is in free solution. The  $\text{UO}_2^{2+}/\text{Cl}^-$  PMF was used to guide our choice of parameters. For this study, we used  $d_0 = 0$ ,  $r_0 = 0.4$  nm,  $n = 12$ , and  $m = 24$ . The coordination number is calculated as a sum over four such switching functions, and therefore takes on values 0 to 4, representing the various actinyl-chloride binding states.

## 2.6 Software Used

Gaussian 09<sup>58</sup> was used for all the QM calculations. Single precision GROMACS-4.5.6 and 5.0.5<sup>59,60</sup> was used for all the molecular dynamics simulations. The SSAGES software suite<sup>61</sup> was used for its ABF implementation. Spatial distribution functions (SDFs) were created using the TRAVIS program.<sup>62</sup> VMD<sup>63</sup> was used for visualization. The PMFs were integrated using MATLAB 2015b. The normalized reactive flux function was calculated using an in-house Python code.

## 3 Results and Discussion

### 3.1 Free Energy Calculations and Stability Constants

The free energy change associated with forming the CIP complex was found to vary greatly by ligand. For example, the activation energy associated with breaking the  $\text{UO}_2/\text{F}^-$  CIP was found to be approximately 78 kJ/mol, but only 24 kJ/mol in the case of  $\text{UO}_2/\text{Cl}^-$ . This disparity is illustrated in Fig. 3.

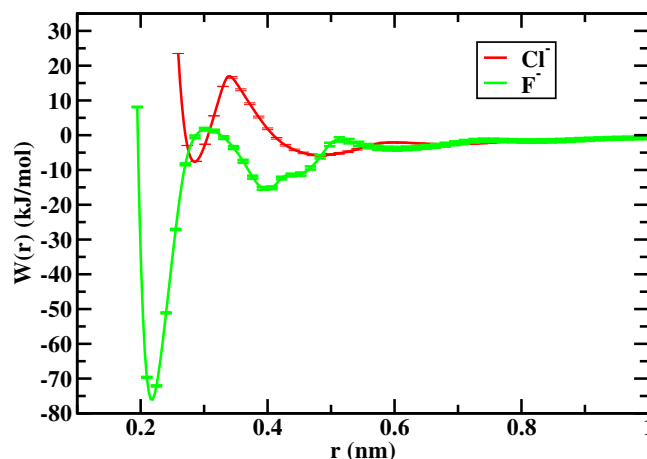


**Fig. 3** PMF plots for  $\text{UO}_2/\text{Cl}^-$  and  $\text{UO}_2/\text{F}^-$  systems, as a function of  $r$ , the actinyl-ligand center of mass distance.

Since both  $\text{F}^-$  and  $\text{Cl}^-$  are monatomic, monovalent anions, but exhibited significantly different binding affinity, a parametric study was performed to investigate the effect of various force field parameters on the strength of ligand binding. In particular, the  $\sigma$  and  $\epsilon$  parameters corresponding to the ligand were varied. It was found that the binding energy has a strong dependence on the  $\sigma$  parameter, which controls the ionic radius, and is rather insensitive to  $\epsilon$ , which controls the strength of attractive dispersion interactions. The PMFs generated from this study can be found in the SI.

The  $\text{CO}_3^{2-}$  and  $\text{SO}_4^{2-}$  systems have two similar configurations that correspond to the CIP. These two configurations are shown for the  $\text{UO}_2/\text{SO}_4^{2-}$  system in Fig. 6. The monodentate configuration, located at 0.383 nm separation, corresponds to a single oxygen of the sulfate interacting with the uranyl cation. As the ligand is brought closer, the sulfate ion will rotate such that two oxygens can coordinate with the uranyl, and a stable bidentate configuration is found at 0.313 nm separation. The bidentate state is less favorable by about 15 kJ/mol.

From the PMFs for each actinyl-ligand system, stability con-

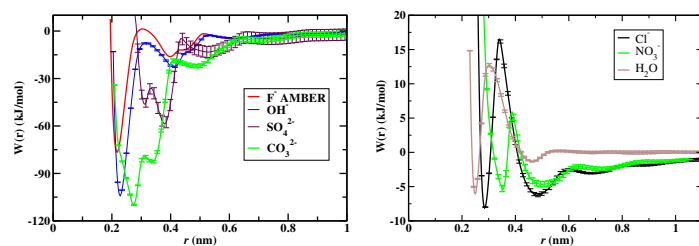


**Fig. 4** PMF plots for interaction between  $\text{UO}_2^{2+}$  and various ligands. Strong ligands are shown on the left, and weak ligands are shown on the right.

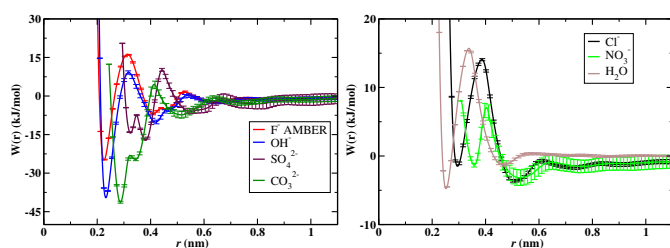


**Fig. 5** PMF plots for interaction between  $\text{NpO}_2^+$  and various ligands.

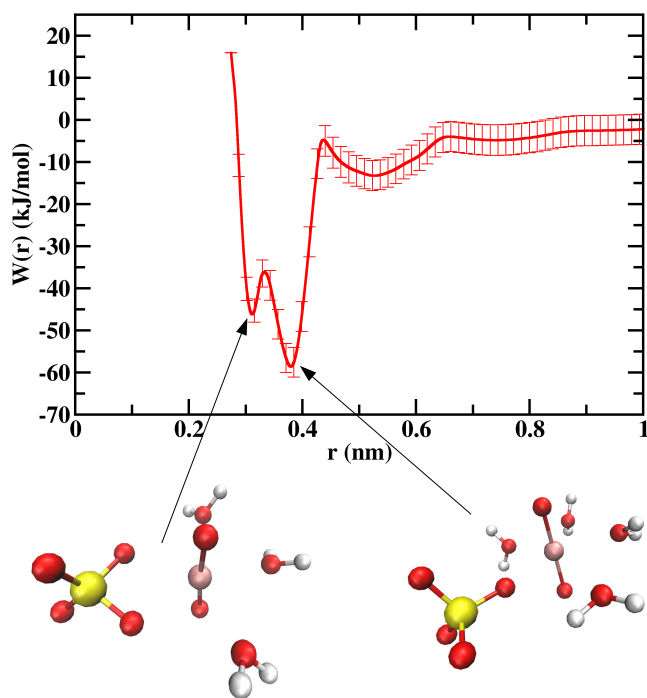


**Fig. 6** PMF plot for  $\text{UO}_2/\text{SO}_4^{2-}$  system. The CIP consists of two configurations, as shown.

stants were calculated, and are shown in Table 2. The ligands are classified according to the strength of their binding with the actinyl ion; strongly interacting ligands bind with energies greater than 50 kJ/mol, while weakly interacting ligands bind on the order of 10 kJ/mol. Highly charged and small ions, like  $\text{F}^-$ ,  $\text{OH}^-$ ,  $\text{CO}_3^{2-}$ ,  $\text{SO}_4^{2-}$  are strongly interacting ligands, whereas  $\text{Cl}^-$ ,  $\text{NO}_3^-$  and water are weakly interacting ligands. Bigger ligands such as  $\text{CO}_3^{2-}$ ,  $\text{SO}_4^{2-}$ , and  $\text{NO}_3^-$  have a larger CIP distance than smaller ligands. Monovalent ligands with a smaller radius such as  $\text{F}^-$  and  $\text{OH}^-$  have a much deeper free energy minimum than larger monovalent ligands and hence make a much stronger CIP complex. This is reflected in the stability constants, shown in Table 2. The constant for the formation of CIP  $K_3$  is the primary contributing factor to overall stability constant  $K_a$  for strongly interacting ligands, whereas SIP and 2SIP contribute primarily towards the association for weakly interacting ligands. Association decreases in the order  $\text{CO}_3^{2-} > \text{OH}^- > \text{F}^- > \text{SO}_4^{2-} > \text{NO}_3^- > \text{Cl}^- > \text{H}_2\text{O}$ . The interaction between  $\text{NpO}_2^+$  and different ligands follow a similar trend for the strong ligands, while the association of the weak ligands decreases in the order  $\text{Cl}^- > \text{H}_2\text{O} > \text{NO}_3^-$ . In addition, association with the monocationic uranyl is weaker.

The trends of stability constants agree well with experimental values, although there isn't quantitative agreement. A number of factors likely contribute to this disagreement. First, the experiments were performed at a finite actinyl/ligand concentration, and the results were corrected using specific ion theory (SIT) to calculate infinite-dilution association constants. Our calculations were performed with a single actinyl-ligand ion pair, which corresponds to approximately 0.05 M. Secondly, actinyl/ligand speciation and association constants are highly sensitive to pH. For example, it has been experimentally demonstrated<sup>65</sup> that  $\text{UO}_2^{2+}/\text{CO}_3^{2-}$  do not form complexes at very high pH. As the pH is reduced to approximately 5,  $\text{UO}_2(\text{CO}_3)$  complexes are the dominant species in solution. At pH values of 6 and 8,  $\text{UO}_2(\text{CO}_3)_2^{2-}$  and  $\text{UO}_2(\text{CO}_3)_3^{4-}$  become the dominant species. Our simulations have an undefined pH, since our water model does not incorporate autoionization. Thus, the key finding is that the relative trends are captured, and association constants are predicted for ligands for which no experimental data exist.

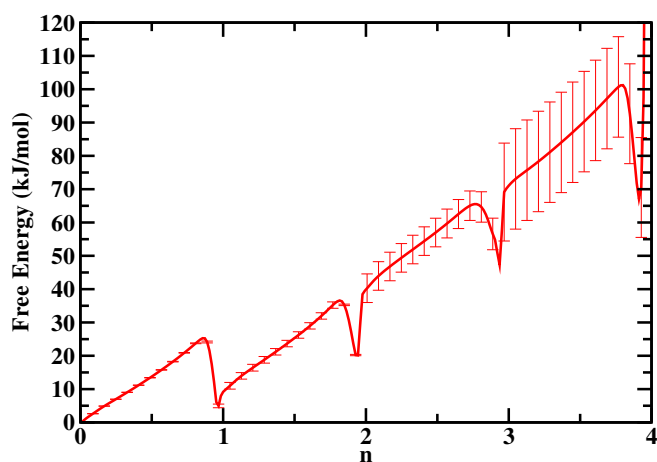
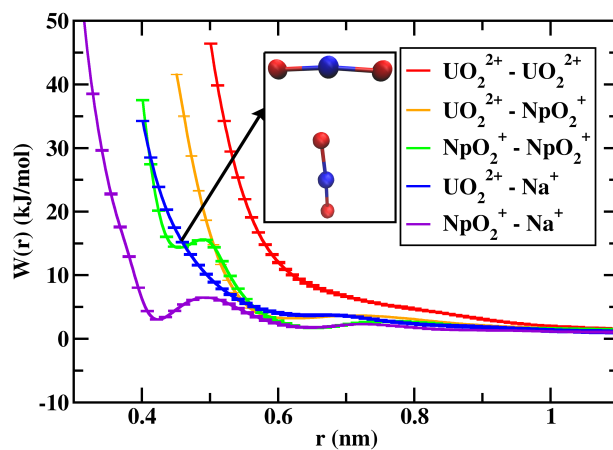
To demonstrate the polyionic association,  $\text{Cl}^-$  ions were gradually added to  $\text{UO}_2^{2+}$  to form the  $[\text{UO}_2\text{Cl}_n]^{2-n}-\text{Cl}^-$  complex, where  $n$  is the actinyl-ligand coordination number, equal to 0, 1, 2, 3, or 4. The free energy as a function of actinyl coordination number is shown in Fig. 7. The free energy change from  $n = 0$  to  $n = 1$  is in good agreement with the PMF shown in Fig 4, without the entropy correction. The addition of the first chloride induces a free energy change of about 5 kJ/mol. It can be seen that the addition of each chloride ion gets more and more difficult as  $n$  increases. Therefore, it can be concluded that the uranyl dication prefers to be completely solvated by water in the presence of chlorides. The  $n = 3$  and 4 states were particularly difficult to sample, so the error is large compared to the other states.

The PMF plots for the cation-cation interactions (CCIs) are shown in Fig. 8. Two small cations electrostatically strongly repel in the gas phase, but in the aqueous phase, the dielectric shielding of water allows some room for association between the two

**Table 2** Stability constants ( $K_a$ ) for  $\text{AnO}_2^{n+} + \text{L}^{m-} \xrightleftharpoons{K_a} [\text{AnO}_2 \cdots \text{L}]^{n-m}$  in the aqueous phase

Ligand	$K_1$	$K_2$	$\log_{10} K_3$	$\log_{10} K_a$		Reference
				Present work	Experiments	
$\text{UO}_2^{2+}$						
$\text{F}^-$ (AMBER)	$2.61 \pm 0.01$	$12.69 \pm 0.05$	$9.5 \pm 0.1$	$10.09 \pm 0.02$	$5.16 \pm 0.06$	35
$\text{F}^-$ (OPLS)	$2.72 \pm 0.03$	$6.16 \pm 0.07$	$8.1 \pm 0.2$	$9.27 \pm 0.02$		
$\text{OH}^-$	$2.983 \pm 0.003$	$141 \pm 4$	$13.43 \pm 0.02$	$15.071 \pm 0.004$	8.40	35
$\text{CO}_3^{2-}$	$5.34 \pm 0.03$	$171 \pm 7$	$14.32 \pm 0.05$	$17.16 \pm 0.01$	9.7, $10.1 \pm 0.4$	35, 64
$\text{SO}_4^{2-}$	$5.5 \pm 0.7$	$6.5 \pm 0.2$	$6.07 \pm 0.07$	$8.43 \pm 0.07$	$2.9 \pm 0.5$ , $3.35 \pm 0.15$	64, 35
$\text{NO}_3^-$	$2.45 \pm 0.01$	$0.89 \pm 0.01$	$-0.89 \pm 0.01$	$0.639 \pm 0.005$	$0.30 \pm 0.15$	35
$\text{Cl}^-$	$1.994 \pm 0.005$	$0.99 \pm 0.01$	$-0.92 \pm 0.02$	$0.626 \pm 0.005$	$*0.17 \pm 0.02$	35
$\text{H}_2\text{O}$	$0.633 \pm 0.003$	$0.439 \pm 0.001$	$-0.559 \pm 0.005$	$0.019 \pm 0.001$	-	
$\text{NpO}_2^+$						
$\text{F}^-$ (AMBER)	$1.03 \pm 0.02$	$1.18 \pm 0.02$	$1.92 \pm 0.01$	$2.02 \pm 0.01$	-	
$\text{F}^-$ (OPLS)	$1.20 \pm 0.03$	$1.14 \pm 0.02$	$1.63 \pm 0.01$	$1.88 \pm 0.01$		
$\text{OH}^-$	$1.20 \pm 0.01$	$2.7 \pm 0.3$	$4.05 \pm 0.05$	$4.555 \pm 0.003$	$4.7 \pm 0.2$	35
$\text{CO}_3^{2-}$	$1.96 \pm 0.06$	$1.50 \pm 0.05$	$4.68 \pm 0.02$	$5.25 \pm 0.02$	$4.81 \pm 0.15$	35
$\text{SO}_4^{2-}$	$2.3 \pm 0.1$	$0.92 \pm 0.02$	$1.09 \pm 0.01$	$1.545 \pm 0.002$	-	
$\text{NO}_3^-$	$1.12 \pm 0.08$	$0.39 \pm 0.02$	$-2.72 \pm 0.2$	$0.20 \pm 0.02$	-	
$\text{Cl}^-$	$1.12 \pm 0.01$	$0.352 \pm 0.003$	$-1.141 \pm 0.009$	$0.289 \pm 0.004$	-	
$\text{H}_2\text{O}$	$0.863 \pm 0.006$	$0.489 \pm 0.001$	$-0.908 \pm 0.001$	$0.226 \pm 0.002$	-	

\*Not with OECD guidelines

**Fig. 7** Free energy as a function of coordination number,  $n$ , for the  $[\text{UO}_2\text{Cl}_n]^{2-n}-\text{Cl}^-$  complex.**Fig. 8** PMF plots for CClIs. The  $\text{NpO}_2^{2+}-\text{NpO}_2^{2+}$  T-shaped complex is shown above the plot.

cations. Association tends to decrease with the increase in the charges of cations. In particular, the  $\text{NpO}_2^{2+}-\text{NpO}_2^{2+}$  PMF exhibits a minimum at approximately 0.45 nm, corresponding to an association between these two species. Upon analysis of the trajectories, this state corresponds to the two neptunyl cations in a T-shaped configuration, as shown in Fig. 8. This T-shaped  $\text{NpO}_2^{2+}-\text{NpO}_2^{2+}$  configuration at 0.42 nm separation has been observed in X-ray scattering experiments.<sup>66</sup>

The CIP, SIP, 2SIP are either absent or difficult to determine in the case of cation-cation interactions (CCIs), thus only overall sta-

**Table 3** Stability constants for CCIs in the aqueous phase ( $r_3 = 0.887$  nm)

Actinyl-Actinyl	$\log_{10} K_a$
$\text{UO}_2^{2+} - \text{UO}_2^{2+}$	$-0.85 \pm 0.02$
$\text{UO}_2^{2+} - \text{NpO}_2^+$	$-0.29 \pm 0.01$
$\text{UO}_2^{2+} - \text{Na}^+$	$-0.340 \pm 0.009$
$\text{NpO}_2^+ - \text{NpO}_2^+$	$-0.214 \pm 0.008$
$\text{NpO}_2^+ - \text{Na}^+$	$-0.19 \pm 0.03$

bility constants were calculated and shown in Table 3. The order of association for CCIs are  $\text{NpO}_2^+ - \text{Na}^+ > \text{NpO}_2^+ - \text{NpO}_2^+ > \text{UO}_2^{2+} - \text{NpO}_2^+ > \text{UO}_2^{2+} - \text{Na}^+ > \text{UO}_2^{2+} - \text{UO}_2^{2+}$ . Uranyl-uranyl ions with both having +2 charges show no association.

### 3.2 Spatial Distribution Functions

The topologies of the CIP, SIP, and 2SIP can be visualized by generating spatial distribution functions (SDF). SDF plots depicting the CIP, SIP, and 2SIP for the interaction between  $\text{UO}_2^{2+}$  and various ligands are shown in Fig. 9 and 10. SDFs of water are also shown for comparison. SDFs showing CIP, SIP, and 2SIP for  $\text{UO}_2^{2+} - \text{F}^-$  interaction are shown in Fig. 9. The PMFs as well as the SDFs suggest that the CIP distance of  $\text{UO}_2^{2+} - \text{F}^-$  is slightly smaller than that of  $\text{UO}_2^{2+} - \text{water}$  interaction. It also suggests that  $\text{F}^-$  replaces a water molecule from the first solvation shell of uranyl ion to form a CIP.

The SIPs for the association of  $\text{UO}_2^{2+}$  with strongly interacting ligands and weakly interacting ligands showed distinct structures. As can be seen in Figure 10, strongly interacting ligands form a single ring type structure in the equatorial region, whereas weakly interacting ligands form a two ring type structure in the biaxial region. This occurs because the interactions between a weak ligand and  $\text{UO}_2^{2+}$  are not strong enough to displace water from the first solvation shell.

### 3.3 CIP Dissociation Rate Constants

We have calculated the TST rate constants and transmission coefficients of CIP dissociation for both the  $\text{UO}_2^{2+}$  dication and  $\text{NpO}_2^+$  monocation with the anionic ligands and water. The normalized reactive flux associated with  $\text{UO}_2^{2+} - \text{OH}^-$  CIP dissociation is given in Fig. 11. In this case, the plateau value is approximately 0.21, which indicates that the true rate of CIP dissociation is 21% of the TST calculation.

Table 4 gives the calculated rate constants for CIP dissociation. The TST rate constants and transmission coefficients can be found in the SI. Since the free energy associated with forming the CIP complex varies greatly by ligand, so do the rates of ligand exchange. Size and charge contribute most to the rate of ligand exchange. Small, highly charged ions like  $\text{CO}_3^{2-}$ ,  $\text{F}^-$ , and  $\text{OH}^-$  bind tightly to the actinyl ion and exchange slowly. On the other hand, larger ions like  $\text{SO}_4^{2-}$  and  $\text{Cl}^-$  bind more weakly than  $\text{CO}_3^{2-}$  and  $\text{F}^-$ , respectively, giving rise to a faster exchange rate. In addition, anionic ligands exchange more rapidly with monocationic  $\text{NpO}_2^+$  than dicationic  $\text{UO}_2^{2+}$ .

The dynamics of water exchange with actinyl dications has been studied both experimentally and computationally. Experi-

**Table 4** Rate constants for actinyl-ligand CIP dissociation

Ligand	FFP	$k_{\text{UO}_2^{2+}} \text{ (s}^{-1}\text{)}$	$k_{\text{NpO}_2^+} \text{ (s}^{-1}\text{)}$
$\text{F}^-$	AMBER	$8 \times 10^{-2} \pm 2$	$4 \times 10^5 \pm 1.5$
	OPLS	$2 \times 10^0 \pm 1$	$5 \times 10^5 \pm 0.9$
$\text{OH}^-$	Literature	$4 \times 10^{-5} \pm 0.8$	$6 \times 10^3 \pm 0.9$
$\text{CO}_3^{2-}$	Literature	$1 \times 10^{-4} \pm 1.6$	$6 \times 10^3 \pm 0.1$
$\text{SO}_4^{2-}$	Literature	$1 \times 10^2 \pm 0.3$	$9 \times 10^8 \pm 2.5$
$\text{NO}_3^-$	Literature	$9 \times 10^8 \pm 0.6$	$1 \times 10^9 \pm 0.2$
$\text{Cl}^-$	AMBER	$1 \times 10^7 \pm 0.2$	$7 \times 10^9 \pm 0.1$
$\text{H}_2\text{O}$	SPC/E	$7 \times 10^8 \pm 0.1$	$1 \times 10^9 \pm 0.1$

mental studies<sup>67-70</sup> of the rate constant for water exchange with  $\text{UO}_2^{2+}$  range from  $10^4$  to  $10^6 \text{ s}^{-1}$ . In contrast, computational studies<sup>71-73</sup> predict faster exchange dynamics, with rate constants on the order of  $10^8 \text{ s}^{-1}$ . Our calculations predict the  $\text{UO}_2^{2+}$ /water exchange rate to be  $7.3 \times 10^8 \text{ s}^{-1}$ . Interestingly, however, computed coordination numbers and the observed exchange mechanism agree with previous computational and experimental studies. It is also interesting that the fast exchange rate predicted here is consistent with several of the previous theoretical studies that found lower free energy barriers than that measured with NMR.

We provide several possible explanations for these observations. First, the NMR experiments record the exchange between water that is associated with the cation and water that is in the bulk. The simulations all consider the exchange dynamics between the first and second coordination shells of the cation. Even in the second coordination shell, however, water still experiences interactions with the cation and cannot be considered to be residing in "bulk" water. Thus the simulations may only be capturing the first rapid part of the exchange process, while the ultimate exchange with the bulk captured by NMR takes longer time. Another explanation is that the models used in the simulations are simply not sophisticated enough to capture the dynamical exchange process between water and  $\text{UO}_2^{2+}$  and need to be improved. In particular, our model does not incorporate polarization. In a recent study<sup>74</sup> of actinide(III) ions, a nonpolarizable (Lennard-Jones + Coulomb) force field exhibited structural properties that were in agreement with both a polarizable model (Thole). However, the two models showed larger differences in water exchange dynamics. The present study can serve as a benchmark for further studies aimed at systematically improving water-actinide force fields.

## 4 Conclusions

Interactions between  $\text{UO}_2^{2+}$  along with  $\text{NpO}_2^+$  and various ligands in the aqueous phase were studied. PMFs and stability constants from MD simulations were calculated for these interactions. First, force field parameters for the interaction between uranyl ion and the ligands were developed using QM PES fitting. Derived FFPs from QM PES fits were over-attractive, as the ligands were not solvated during QM calculations, yielding a very strong association which are not in agreement with experiments. However, FFPs obtained from the literature and using empirical combining rules were found to better reproduce the association between actinyl

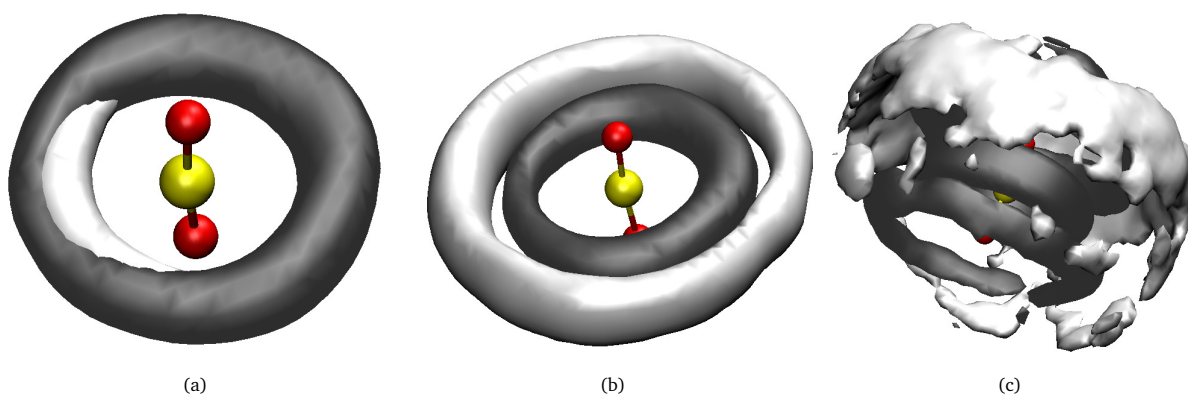


**Fig. 9** SDFs for  $\text{UO}_2^{2+} - \text{F}^-$  (AMBER) (Silver = water, Grey =  $\text{F}^-$ ). (a) CIP located at 0.222 nm, (b) SIP of  $\text{F}^-$  at 0.4 nm, CIP of water. (c) 2SIP of  $\text{F}^-$  at 0.61 nm, SIP of water.

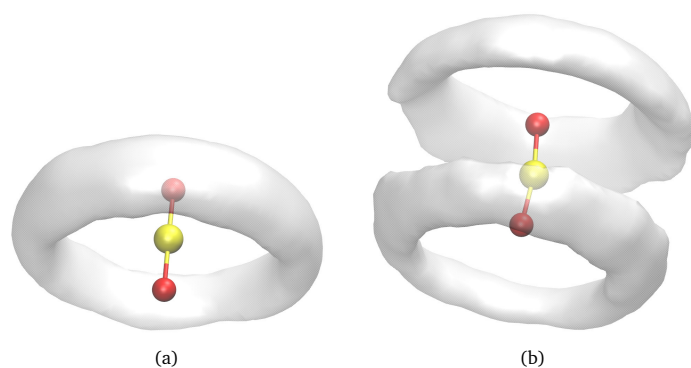


**Fig. 10** Comparison between two different types of SDFs, depicting the 2nd minima (SIP) of PMF plots. (a)  $\text{F}^-$ , a strong ligand, (b)  $\text{Cl}^-$ , a weak ligand.

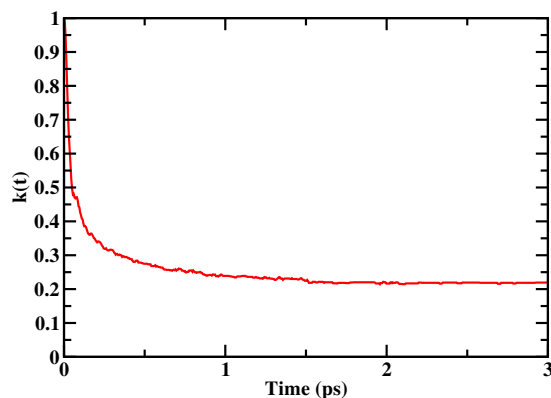


**Fig. 11** The normalized reactive flux,  $k(t)$ , associated with  $\text{UO}_2^{2+} - \text{OH}^-$  CIP dissociation.

ions and ligands, and the values of stability constants were in reasonable agreement with those from the experiments. The trends of stability constants also agreed well with the experiments.

$\text{UO}_2^{2+}$  associated strongly with anionic ligands compared to  $\text{NpO}_2^+$ . Two different types of ligands were identified: strongly interacting and weakly interacting. PMFs of strongly interacting ligands show a much deeper CIP compared to that of weaker interacting ligands. Further, polyionic association was demonstrated by consecutively adding chloride ions to uranyl ion. The subsequent association of chloride ion gets increasingly difficult with the further addition of chloride ions. Furthermore, association between two cations was studied. Neptunyl monocation systems showed a local minimum in the PMF at short distances. Finally, SDFs depicting multi-step ion pairs (CIP, SIP, and 2SIP) were studied. The SIPs of strongly interacting ligands form a single ring type structures, whereas weakly interacting ligands form a two ring type structure.

We also analyzed the kinetics of ligand exchange using the transition state theory formalism. In addition, we corrected this result by calculating the transmission coefficient for each event by performing simulations in the constrained-reaction-coordinate ensemble. All calculated transmission coefficients were found to be less than 0.5, indicating that TST can be a poor approximation where solvent friction is significant. The greatest contribution to the rate of CIP dissociation comes from the free energy barrier, not the effect of barrier recrossing. In addition, the CIP dissociation rates were significantly higher in the case of the monocationic actinyl ion, as opposed to the dicationic form.

In the present work, although we looked only at the speciation of  $\text{UO}_2^{2+}$  and  $\text{NpO}_2^+$  in aqueous phase, we expect that the association behavior and the order of stability constants between ligands and actinyl ions of U, Np, Pu, and Am in their +2 and +1 charged states should be similar to those of  $\text{UO}_2^{2+}$  and  $\text{NpO}_2^+$ , respectively. This comes from the fact that the force field parameters of the divalent and mono-valent actinyl ions are very similar, respectively, as described in our previous work.<sup>20</sup>

## 5 Acknowledgements

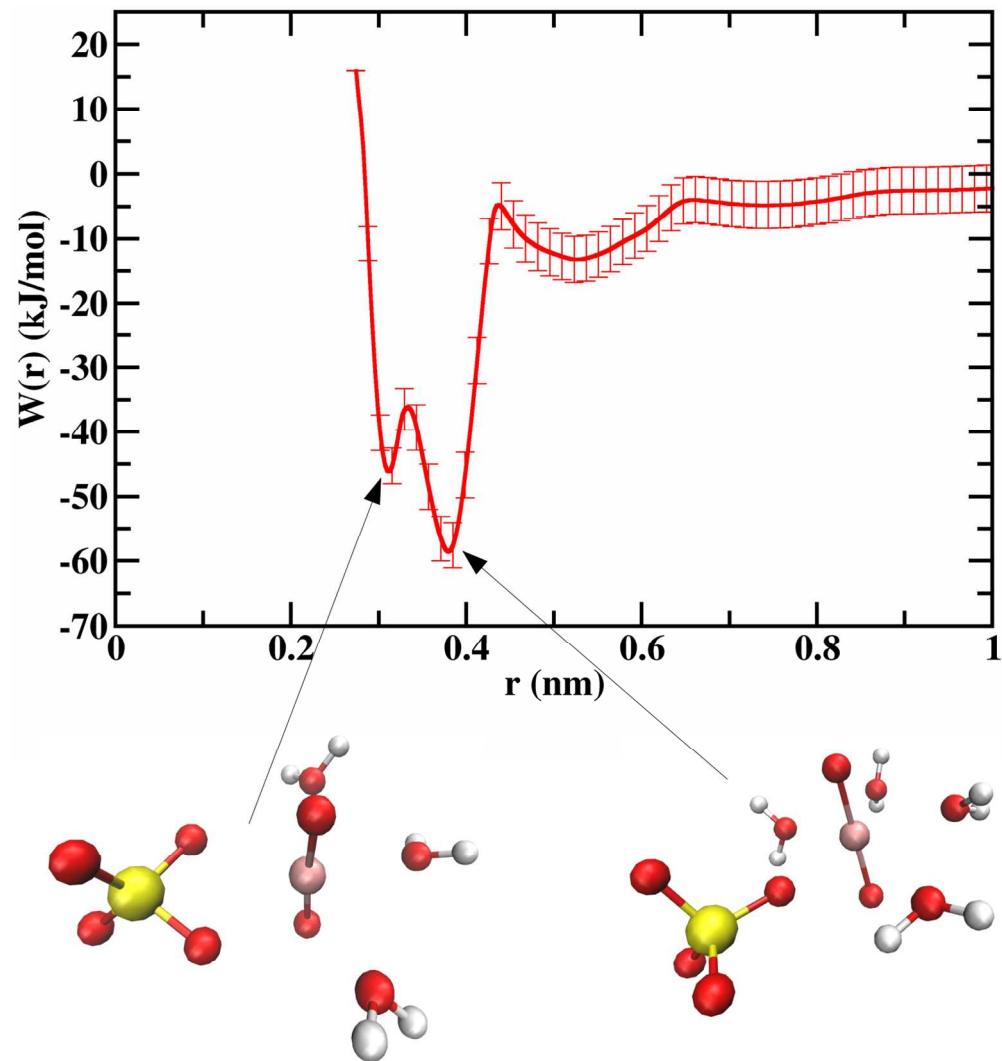
This work was supported as part of the Materials Science of Actinides Energy Frontier Research Center, funded by the U.S. Department of Energy, Office of Science, Basic Energy Sciences under award DE-SC0001089. The authors thank Hythem Sidky for his guidance in performing free energy calculations, as well as countless constructive discussions.

## References

- 1 A. E. Martell and R. D. Hancock, *Metal Complexes in Aqueous Solutions*, Springer Science & Business Media, 2013.
- 2 R. D. Hancock and A. E. Martell, *Chem. Rev.*, 1989, **89**, 1875–1914.
- 3 S. Vukovic, B. P. Hay and V. S. Bryantsev, *Inorg. Chem.*, 2015, 3995–4001.
- 4 G. E. Sigmon, J. Ling, D. K. Unruh, L. Moore-Shay, M. Ward, B. Weaver and P. C. Burns, *J. Am. Chem. Soc.*, 2009, **131**, 16648–16649.
- 5 L. Gagliardi and B. O. J. Roos, *Inorg. Chem.*, 2002, **41**, 1315–1319.
- 6 M. Bühl, N. Sieffert, A. Chaumont and G. Wipff, *Inorg. Chem.*, 2011, **50**, 299–308.
- 7 M. Bühl, N. Sieffert, V. Golubnychiy and G. Wipff, *J. Phys. Chem. A*, 2008, **112**, 2428–2436.
- 8 M. Bühl, N. Sieffert and G. Wipff, *Chem. Phys. Lett.*, 2009, **467**, 287–293.
- 9 M. Bühl, G. Schreckenbach, N. Sieffert and G. Wipff, *Inorg. Chem.*, 2009, **48**, 9977–9979.
- 10 M. Bühl and H. Kabrede, *Inorg. Chem.*, 2006, **45**, 3834–6.
- 11 M. Bühl, R. Diss and G. Wipff, *Inorg. Chem.*, 2007, **46**, 5196–206.
- 12 M. Bühl and G. Wipff, *ChemPhysChem*, 2011, **12**, 3095–3105.
- 13 S. O. Odoh and G. Schreckenbach, *Inorg. Chem.*, 2013, **52**, 5590–5602.
- 14 V. Vallet, U. Wahlgren and I. Grenthe, *J. Phys. Chem. A*, 2012, **116**, 12373–12380.
- 15 X. Ye, R. B. Smith, S. Cui, V. de Almeida and B. Khomami, *Solvent Extraction and Ion Exchange*, 2010, **28**, 1–18.
- 16 C. Gaillard, A. Chaumont, I. Billard, C. Hennig, A. Ouadi and G. Wipff, *Inorg. Chem.*, 2007, **46**, 4815–4826.
- 17 P. Guilbaud and G. Wipff, *J. Mol. Struct. THEOCHEM*, 1996, **366**, 55–63.
- 18 L. X. Dang, Q. N. Vo, M. Nilsson and H. D. Nguyen, *Chemical Physics Letters*, 2017, **671**, 58–62.
- 19 N. Rai, S. P. Tiwari and E. J. Maginn, *J. Phys. Chem. B*, 2012, **116**, 10885–10897.
- 20 V. Pomogaev, S. P. Tiwari, N. Rai, G. S. Goff, W. Runde, W. F. Schneider and E. J. Maginn, *Phys. Chem. Chem. Phys.*, 2013, **15**, 15954–63.
- 21 S. P. Tiwari, N. Rai and E. J. Maginn, *Phys. Chem. Chem. Phys.*, 2014, **16**, 8060–8069.
- 22 S. P. Tiwari, *PhD thesis*, University of Notre Dame, 2015.
- 23 E. Darve, D. Rodríguez-Gómez and A. Pohorille, *Journal of Chemical Physics*, 2008, **128**, 1–13.
- 24 E. Carter, G. Ciccotti, J. T. Hynes and R. Kapral, *Chem. Phys. Lett.*, 1989, **156**, 472–477.
- 25 H. J. C. Berendsen, J. R. Grigera and T. P. Straatsma, *J. Phys. Chem.*, 1987, **91**, 6269–6271.
- 26 M. P. Allen and D. J. Tildesley, *Computer Simulation of Liquids*, Clarendon Press: Oxford, 1987.
- 27 J. Kirkwood, *J. Chem. Phys.*, 1935, **3**, 300.
- 28 B. Roux, *Comput. Phys. Commun.*, 1995, **91**, 275–282.
- 29 C. J. Fennell, A. Bizjak, V. Vlachy and K. A. Dill, *J. Phys. Chem. B*, 2009, **113**, 6782–6791.
- 30 J. S. Hub, B. L. de Groot and D. van der Spoel, *J. Chem. Theory Comput.*, 2010, **6**, 3713–3720.
- 31 D. Chandler, *J. Chem. Phys.*, 1978, **68**, 2959.
- 32 D. Frenkel and B. Smit, *Understanding Molecular Simulation From Algorithms to Applications*, Academic Press, New York, 2002.
- 33 T. Darden, D. York and L. Pedersen, *J. Chem. Phys.*, 1993, **98**, 10089–10092.
- 34 U. Essmann, L. Perera, M. L. Berkowitz, T. Darden, H. Lee and L. G. Pedersen, *J. Chem. Phys.*, 1995, **103**, 8577.
- 35 R. Guillaumont and F. J. Mompean, *Update on the Chemical Thermodynamics of Uranium, Neptunium, Plutonium, Americium and Technetium*, Elsevier Amsterdam, 2003.
- 36 L. G. Sillén, A. E. Martell and J. Bjerrum, *Stability Constants of Metal-Ion Complexes*, Chemical Society London, 1964, vol. 17.
- 37 Y. Marcus and G. Hefter, *Chem. Rev.*, 2006, **106**, 4585–621.
- 38 N. K. Bjerrum, *Dan. Vidensk. Selsk.*, 1926, **7**, 9.
- 39 A. A. Chialvo, P. T. Cummings, H. D. Cochran, J. M. Simonson and R. E. Mesmer, *J. Chem. Phys.*, 1995, **103**, 9379.
- 40 R. P. Matthews and K. J. Naidoo, *J. Phys. Chem. B*, 2010, **114**, 7286–7293.
- 41 R. Buchner, T. Chen and G. Hefter, *J. Phys. Chem. B*, 2004, **108**, 2365–2375.
- 42 E. Guardia and J. A. Padró, *J. Phys. Chem.*, 1990, **94**, 6049–6055.
- 43 K. J. Naidoo, A. S. Lopis, A. N. Westra, D. J. Robinson and K. R. Koch, *J. Am. Chem. Soc.*, 2003, **125**, 13330–13331.
- 44 B. Hess, C. Holm and N. van der Vegt, *J. Chem. Phys.*, 2006, **124**, 164509.
- 45 W. B. Russel, D. A. Saville and W. R. Schowalter, *Colloidal Dispersions*, Cambridge University Press, 1989, p. 102.
- 46 A. Alexander P. Lyubartsev and Laaksonen, *Phys. Rev. E*, 1995, **52**, 3730–3737.
- 47 M. Ullner, C. E. Woodward and B. Jönsson, *J. Chem. Phys.*, 1996, **105**, 2056.
- 48 Y. Wu, H. L. Tepper and G. A. Voth, *J. Chem. Phys.*, 2006, **124**, 24503.
- 49 R. Rey and J. T. Hynes, *J. Phys. Chem.*, 1996, **100**, 5611–5615.
- 50 O. A. Karim and J. McCammon, *Chem. Phys. Lett.*, 1986, **132**, 219–224.
- 51 T. S. van Erp and P. G. Bolhuis, *Journal of Computational Physics*, 2004, **205**, 157–181.

- 52 G. Ciccotti, M. Ferrario, J. T. Hynes and R. Kapral, *Chem. Phys.*, 1989, **129**, 241–251.
- 53 G. Ciccotti, M. Ferrario, J. T. Hynes and R. Kapral, *J. Chem. Phys.*, 1990, **93**, 7137–7147.
- 54 R. Rey and E. Guardia, *J. Phys. Chem.*, 1992, **96**, 4712–4718.
- 55 S. Kerisit and C. Liu, *J. Phys. Chem. A*, 2013, **117**, 6421–6432.
- 56 G. Fiorin, M. L. Klein and J. Hénin, *Molecular Physics*, 2013, **111**, 3345–3362.
- 57 T. Ikeda, M. Hirata, T. Kimura, T. Ikeda, M. Hirata and T. Kimura, 2012, **244507**, year.
- 58 M. J. Frisch et al., *Gaussian 09 Revision B.1*.
- 59 B. Hess, C. Kutzner, D. van der Spoel and E. Lindahl, *J. Comput. Theor. Chem.*, 2008, **4**, 435–447.
- 60 D. Van Der Spoel, E. Lindahl, B. Hess, G. Groenhof, A. E. Mark and H. J. C. Berendsen, *J. Comput. Chem.*, 2005, **26**, 1701–1718.
- 61 H. Sidky, Y. J. Colãşn, J. Helfferich, B. J. Sikora, C. Bezik, W. Chu, F. Giberti, A. Z. Guo, X. Jiang, J. Lequieu, J. Li, J. Moller, M. J. Quevillon, M. Rahimi, H. Ramezani-Dakhel, V. S. Rathee, D. R. Reid, E. Sevgen, V. Thapar, M. A. Webb, J. K. Whitmer and J. J. de Pablo, *The Journal of Chemical Physics*, 2018, **148**, 044104.
- 62 M. Brehm and B. Kirchner, *J. Chem. Inf. Model.*, 2011, **51**, 2007–23.
- 63 W. Humphrey, A. Dalke and K. Schulten, *J. Mol. Graph.*, 1996, **14**, 33–38.
- 64 R. J. Lemire and P. R. Tremaine, *Journal of Chemical & Engineering Data*, 1980, **25**, 361–370.
- 65 D. Langmuir and C.-K. D. Hsi, 1985, 1931–1941.
- 66 S. Skanthakumar, M. R. Antonio and L. Soderholm, *Inorganic Chemistry*, 2008, **47**, 4591–4595.
- 67 N. Bardin, P. Rubini and C. Madic, *Radiochim. Acta*, 1998, **83**, 189–194.
- 68 Y. Ikeda, S. Soya, H. Fukutomi and H. Tomiyasu, *J. Inorg. Nucl. Chem.*, 1979, **41**, 1333–1337.
- 69 Farkas, Ildikó and Bányai, István and Szabó, Zoltán and Wahlgren, Ulf and Grenthe Ingmar, *Inorg. Chem.*, 2000, **39**, 799–805.
- 70 Z. Szabó, J. Glaser and I. Grenthe, *Inorg. Chem.*, 1996, **35**, 2036–2044.
- 71 V. Vallet, U. Wahlgren, B. Schimmelpfennig, Z. Szabó and I. Grenthe, *J. Am. Chem. Soc.*, 2001, **123**, 11999–2008.
- 72 S. Kerisit and C. Liu, *Geochim. Cosmochim. Acta*, 2010, **74**, 4937–4952.
- 73 D. Hagberg, G. Karlström, B. O. Roos and L. Gagliardi, *J. Am. Chem. Soc.*, 2005, **127**, 14250–14256.
- 74 R. Spezia, V. Migliorati and P. D'Angelo, *The Journal of Chemical Physics*, 2017, **147**, 161707.

MD simulations are used to explore the thermodynamics of actinyl-ligand binding in water.



564x598mm (72 x 72 DPI)